



HAL
open science

Mitochondrial impairment induced by postnatal ActRIIB blockade does not alter function and energy status in exercising mouse glycolytic muscle in vivo

Nelly Béchir, Émilie Pecchi, Karima Relizani, Christophe Vilmen, Yann Le Fur, Monique Bernard, Helge Amthor, David Bendahan, Benoit Giannesini

► To cite this version:

Nelly Béchir, Émilie Pecchi, Karima Relizani, Christophe Vilmen, Yann Le Fur, et al.. Mitochondrial impairment induced by postnatal ActRIIB blockade does not alter function and energy status in exercising mouse glycolytic muscle in vivo. *AJP - Endocrinology and Metabolism*, 2016, 310 (7), pp.E539-E549. 10.1152/ajpendo.00370.2015 . hal-03548290

HAL Id: hal-03548290

<https://hal.science/hal-03548290>

Submitted on 1 Feb 2022

HAL is a multi-disciplinary open access archive for the deposit and dissemination of scientific research documents, whether they are published or not. The documents may come from teaching and research institutions in France or abroad, or from public or private research centers.

L'archive ouverte pluridisciplinaire **HAL**, est destinée au dépôt et à la diffusion de documents scientifiques de niveau recherche, publiés ou non, émanant des établissements d'enseignement et de recherche français ou étrangers, des laboratoires publics ou privés.

Mitochondrial impairment induced by postnatal ActRIIB blockade does not alter function and energy status in exercising mouse glycolytic muscle in vivo

Nelly BÉCHIR¹, Émilie PECCHI¹, Karima RELIZANI², Christophe VILMEN¹, Yann LE FUR¹,
Monique BERNARD¹, Helge AMTHOR², David BENDAHAN¹, Benoît GIANNESINI¹

¹ *Aix-Marseille Université, CNRS, CRMBM UMR 7339, 13385, Marseille, France*

² *Université de Versailles Saint-Quentin-en-Yvelines, UFR des sciences de la santé, INSERM U1179, LIA BAHN CSM, SQY Therapeutics, 78180 Montigny-le-Bretonneux, France;*

Running head: Metabolic and functional impacts of ActRIIB blockade

Correspondence: Benoît GIANNESINI
Centre de Résonance Magnétique Biologique et Médicale (CRMBM),
UMR 7339 CNRS – Aix-Marseille Université
Faculté de Médecine de Marseille
27 Bd Jean Moulin, 13385 Marseille, Cedex 05
E-mail : benoit.giannesini@univ-amu.fr

ABSTRACT

Because it leads to a rapid and massive muscle hypertrophy, postnatal blockade of the activin type IIB receptor (ActRIIB) is a promising therapeutic strategy for counteracting muscle wasting. However, the functional consequences remain very poorly documented *in vivo*. Here, we have investigated the impact of 8-week ActRIIB blockade with soluble receptor (sActRIIB-Fc) on gastrocnemius muscle anatomy, energy metabolism and force-generating capacity in wild-type mice using totally noninvasive magnetic resonance (MR) imaging and dynamic 31-phosphorus MR spectroscopy. Compared to vehicle (PBS) control, sActRIIB-Fc treatment resulted in a dramatic increase in body weight (+29%) and muscle volume (+58%) calculated from hindlimb MR imaging, but did not alter fiber-type distribution determined via myosin heavy chain isoforms analysis. In resting muscle, sActRIIB-Fc treatment induced acidosis and PCr depletion, thereby suggesting reduced tissue oxygenation. During an *in vivo* fatiguing exercise (6-min of repeated maximal isometric contraction electrically-induced at a frequency of 1.7 Hz), maximal and total absolute forces were larger in sActRIIB-Fc treated animals (+26% and +12%, respectively) whereas specific force and fatigue resistance were lower (-30% and 37%, respectively). Treatment with sActRIIB-Fc further decreased the maximal rate of oxidative ATP synthesis (-42%) and the oxidative capacity (-34%), but did not alter the bioenergetics status in contracting muscle. Our findings demonstrate *in vivo* that sActRIIB-Fc treatment increases absolute force-generating capacity and reduces mitochondrial function in glycolytic gastrocnemius muscle, but this reduction does not compromise energy status during sustained activity. Overall, these data support the clinical interest of postnatal ActRIIB blockade.

Keywords: Skeletal muscle hypertrophy; Activin type IIB receptor; Myostatin; Force; Fatigue.

INTRODUCTION

ActRIIB is a transmembrane serine-threonine kinase receptor highly expressed in mammalian skeletal muscle. It mediates signaling for myostatin (GDF8) and other members of the transforming growth factor β family that are involved in the negative regulation of skeletal muscle development (16, 37). Disruption of the ActRIIB signaling pathway leads to a rapid and massive increase in muscle mass resulting from fiber hypertrophy with increased myofiber protein synthesis (10, 58). In that context, several pharmacological approaches based on the postnatal ActRIIB signaling blockade have been considered for counteracting muscle wasting commonly associated to ageing, neuromuscular disorders and various catabolic diseases (17, 33, 38). These approaches mainly include the systemic delivery of neutralizing antibodies against ActRIIB or myostatin (31, 36), and injection of a soluble recombinant form of ActRIIB (sActRIIB-Fc), which acts as a decoy receptor disrupting the interaction of endogenous ActRIIB receptor with its ligands (5, 38, 44).

Although ActRIIB signaling blockade has been already tested in patients (30, 57) and animal models (10, 44, 47) suffering from dystrophic and neurological disorders, it is noteworthy that the impact of such a blockade has been very poorly documented in healthy muscle *in vivo*. This issue is however an important prerequisite for a better understanding of the effects of ActRIIB blockade in diseased muscle. It has been shown that postnatal disruption of the ActRIIB signaling in normal mice improves functional parameters such as grip strength (1, 33) and absolute force in isolated muscle (1, 15), but on the other hand decreases the resistance to fatigue (15, 52). These results are in all respects comparable to those obtained in myostatin-deficient mice in which the improved force has been documented (2, 19, 43, 45) and the increased fatigability has been assigned to a mitochondrial impairment evidenced on the basis of *in vitro* assays (45, 48) and *in vivo* ^{31}P -MRS measurements (6, 19). Interestingly, long-term sActRIIB-Fc treatment in wild-type mice has been shown to reduce the expression of oxidative phosphorylation genes (50, 52, 60) as well as the level of porin, an outer mitochondrial membrane protein involved in ATP transport between the cytosol and the

mitochondrial matrix (52). These findings suggest that ActRIIB blockade negatively affects the muscle mitochondrial function, which could have undesirable clinical consequences. Nevertheless, this potent impairment has been so far assessed only through in vitro experiments, and the corresponding effects on energetics and mechanical performance in exercising muscle are then missing in vivo.

The aim of the current study was to investigate strictly noninvasively the impact of long-term ActRIIB signaling blockade on gastrocnemius muscle anatomy, energy metabolism and mechanical performance in wild-type mice. We intended especially to clarify (i) whether ActRIIB signaling blockade impairs mitochondrial function similarly to what has been reported in myostatin-deficient mice, and (ii) whether bioenergetics and force-generating capacity during a fatiguing bout of exercise are impaired under these conditions. Functional investigations were performed in electrostimulated muscle in vivo using MR imaging and ³¹P-MR spectroscopy (³¹P-MRS) while the electrophoretic separation of myosin heavy-chain (MHC) isoforms provided information about the fiber type composition.

MATERIALS AND METHODS

Animal care and feeding

Sixteen C57BL/6 3-month old mice (Janvier Labs, Le Genest Saint Isle, France) were used for these experiments conducted in strict accordance with the guidelines of the European Communities Council Directive 86/609/EEC for Care and Use of Laboratory Animals. All animal experiments were performed according to protocols reviewed and approved by the Institutional Animal Care Committee of Aix-Marseille University (permit number 93-21122012) and under the supervision of BG (license number 13.164 2008/11/25). Every attempt was made to minimize the number and the suffering of animals. Mice were socially housed as four per cage in an environmentally controlled facility (12-12 h light-dark cycle, 22°C) with free

access to commercial standard food and water until the time of experiment. After experiments, animals were euthanized by cervical dislocation following isoflurane anesthesia. Gastrocnemius muscles were immediately removed, freeze-clamped with nitrogen-chilled metal tongs, and stored at -80°C for in vitro measurements. For each mouse, the delay between euthanasia and muscle freeze clamping was less than 20 s.

Experimental design

The postnatal blockade of ActRIIB signaling pathway was achieved using a soluble fusion protein (sActRIIB-Fc, also called RAP-031, Acceleron Pharma Inc., Cambridge, MA, USA) generated by fusing the ActRIIB extracellular domain to the mouse immunoglobulin Fc region (44). Mice were assigned to two groups ($n = 8$ per group) of comparable mean body weights. For a total of 8 weeks, animals were injected subcutaneously twice weekly with either sActRIIB-Fc (10 mg/kg body weight) or an equal volume of vehicle (10 mM PBS; control group).

Noninvasive investigation of gastrocnemius muscle function and energetics

Each animal was tested twice over a one-week period in order to evaluate strictly noninvasively bioenergetics, anatomy and force-generating capacity in electrostimulated gastrocnemius muscle. During the first testing session, MR imaging measurements were performed to get information about muscle volume, and metabolic changes associated to muscle activity were investigated using ^{31}P -MR spectroscopy throughout a standardized 6-min fatiguing exercise. During the second session, gastrocnemius muscle was electrostimulated with trains of incremental frequencies (1-150 Hz) and the corresponding force was measured.

Animal preparation. Mice were initially anesthetized in an induction chamber using 1.75% isoflurane in 33% O₂ (0.2 L/min) and 66% N₂O (0.4 L/min). The left hindlimb was shaved before an electrode cream was applied at the knee and heel regions to optimize transcutaneous electrostimulation. Anesthetized animal was placed supine in a home-built

cradle which has been especially designed for the strictly noninvasive MR investigation of gastrocnemius muscle function (20). This muscle was chosen because it is easily accessible for MR measurements and preferentially activated using our experimental methodology. The cradle integrates an ergometer consisting of 9 x 24 mm foot pedal coupled to a force transducer constructed by sticking a strain gauge (120-ohm internal resistance; ref 1-LY11-6/120A, HBM GmbH, Darmstadt, Germany) on a Bakelite slat (0.4 mm thickness) in a Wheatstone bridge design (3 × 120 ohm). The animal's foot was positioned on the pedal of the ergometer and the lower hindlimb was centered inside a 20-mm-diameter ¹H Helmholtz imaging coil while the belly of the gastrocnemius muscle was located above an elliptic (8 x 12 mm²) ³¹P-MRS surface coil. Corneas were protected from drying by applying ophthalmic cream, and animal's head was placed in a home-built facemask continuously supplied with 1.75% isoflurane in 33% O₂ (0.2 L/min) and 66% N₂O (0.4 L/min). Body temperature was controlled and maintained at a physiological level throughout the experiment using a feedback loop including an electrical heating blanket, a temperature control unit (ref. 507137, Harvard Apparatus, Holliston, MA, USA) and a home-built rectal thermometer.

Muscle electrostimulation procedure and force output measurement. Muscle contractions were achieved by transcutaneous electrostimulation using two rod-shaped 1.5-mm-diameter electrodes integrated in the experimental cradle and connected to a constant-current stimulator (DS7A, Digitimer, Hertfordshire, United Kingdom). One electrode was placed at the heel level and the other one was located just above the knee joint. Electrical signal coming out from the force transducer was amplified (Operational amplifier AD620, Analog Devices, Norwood, MA, USA; 70-dB gain; 0-5 kHz bandwidth) and converted to a digital signal (PCI-6220, National Instrument, Austin, TX, USA) that was continuously monitored and recorded on a personal computer using the WinATS software version 6.5 (Sysma, Aix-en-Provence, France).

Preliminary adjustments. Before each experiment, muscle was passively stretched at rest by adjusting the angle between the foot and the lower hindlimb in order to produce maximal isometric twitch amplitude in response to supramaximal square wave pulses (1-ms

duration). The individual maximal electrostimulation intensity was determined by progressively increasing the stimulus intensity until there was no further peak twitch force increase.

Fatigue exercise and force-frequency protocol. The fatiguing exercise was performed simultaneously to the dynamic ^{31}P -MRS acquisition. It consisted in 6 min of repeated maximal isometric contractions induced electrically at a frequency of 1.7 Hz. Absolute force production (expressed as force-time integral, in N*s) was calculated by integrating the isometric force (in N) with respect to time. During the force-frequency protocol, gastrocnemius muscle was electrostimulated with trains (0.75 sec duration; rest interval of 30 sec) of incremental frequencies (1, 10, 20, 30, 50, 75, 100, and 150 Hz) and the corresponding force data were processed as followed: The isometric peak force was measured for each train and the overall dataset was fitted to the Hill equation for calculating f_{50} , i.e., the electrostimulation frequency for which 50% of the maximal force was exerted. Specific force was calculated by normalizing the absolute force with the gastrocnemius muscle volume quantified from hindlimb MR images (see below).

MR data acquisition and processing. Explorations were performed in the 4.7-Tesla horizontal magnet of a 47/30 Biospec Avance MR system (Bruker, Karlsruhe, Germany) equipped with a Bruker 120-mm BGA12SL (200 mT/m) gradient insert. Ten consecutive noncontiguous 0.5-mm spaced axial slices (1-mm thickness) covering the region from the knee to the ankle were selected across the lower hindlimb. RARE images of these slices (8 echoes; effective echo time = 67.9 ms; actual echo time = 16.7 ms; 2000-ms repetition time; one accumulation; 20 x 15 mm field of view; 256 x 256 matrix size) were recorded at rest. ^{31}P -MR spectra (8 kHz sweep width; 2048 data points) from the gastrocnemius region were continuously acquired at rest (6 min), during the 6-min fatiguing exercise and during the following 15-min of recovery period. MR data acquisition was gated to muscle electrostimulation in order to reduce potential motion artifacts due to contraction. A fully relaxed spectrum (12 scans, 20-s repetition time) was acquired at rest, followed by a total of 768 saturated free induction decays (FID) (1.875 s repetition time). The first 64 FIDs were acquired at rest and summed together. The next 192 FIDs were acquired during the fatiguing

exercise and were summed by packets of 32, allowing a 60-s temporal resolution. The remaining 512 FIDs were obtained during the postexercise recovery period and were summed as 7 packets of 32 FIDs followed by 3 packets of 64 FIDs (120-s temporal resolution) and one packet of 96 FIDs (160-s temporal resolution).

MR data were processed using custom-written analysis programs developed under the IDL (Interactive Data Language, Exelis Visual Information Solutions, Boulder, CO, USA) environment (35, 40). For each MR image, region of interest was manually outlined so that the corresponding cross sectional area of the gastrocnemius muscle was measured. Muscle volume was calculated by summing the volumes between consecutive slices. Relative concentrations of phosphocreatine (PCr), inorganic phosphate (P_i) and ATP were obtained from ^{31}P -MR spectra by a time-domain fitting routine using the AMARES-MRUI Fortran code (56) and appropriate prior knowledge for the ATP multiplets. Absolute amounts of phosphorylated compounds were expressed relative to a resting ATP concentration determined in vitro using a bioluminescence-based method (see below), and intracellular pH was calculated from the chemical shift of the P_i signal relative to PCr (3). ADP concentration was calculated from [PCr], [ATP] and pH considering the equilibrium constant ($K = 1.67 \cdot 10^9 \text{ M}^{-1}$) of the creatine kinase (CK) reaction (53). $V\text{PCr}_{\text{stim}}$ (the initial rate of PCr degradation at the start of the fatiguing exercise, in mM/min) was calculated as the product of k_{stim} (the pseudo-first-order rate-constant of PCr degradation) and $[\text{PCr}]_{\text{cons}}$ (the amount of PCr consumed at the end of the exercise). The constant k_{stim} was determined by fitting with a least mean-squared algorithm the time-course of PCr degradation to a single exponential curve described by the equation: $[\text{PCr}]_t = [\text{PCr}]_{\text{end}} + [\text{PCr}]_{\text{cons}} \cdot e^{-kt}$, where $[\text{PCr}]_{\text{end}}$ is the concentration of PCr measured at the end of the exercise. Similarly, $V\text{PCr}_{\text{rec}}$ (the initial rate of PCr resynthesis at the start of the recovery period following the fatiguing exercise, in mM/min) was calculated as the product of k_{rec} (the pseudo-first-order rate-constant of PCr resynthesis) and $[\text{PCr}]_{\text{cons}}$. In order to determine k_{rec} , the PCr time-course during the recovery period was fitted with a least mean-squared algorithm to a single exponential curve described by the equation: $[\text{PCr}]_t = [\text{PCr}]_{\text{rest}} - [\text{PCr}]_{\text{cons}} \cdot e^{-kt}$, where $[\text{PCr}]_{\text{rest}}$ is the concentration of PCr measured at rest. The maximal rate of

oxidative ATP synthesis (Q_{\max} , mM/min) was calculated using $VPCr_{\text{rec}}$ and the level of ADP measured at the end of the fatiguing exercise as previously described (28): $Q_{\max} = (1+K_m/[ADP]_{\text{end}})VPCr_{\text{rec}}$ where K_m (the apparent Michaelis-Menten constant of mitochondrial respiration for ADP, i.e., the ADP concentration at half-maximal rate of oxidative ATP synthesis) is 30 μM in mouse gastrocnemius muscle (29). The rate of proton efflux from the muscle (in mM/min) was calculated in the early stage of the postexercise recovery period from the changes in pH and levels of high-energy phosphorylated contents as described previously (19, 28). PCr cost of contraction (PCr_{cost} , in $\mu\text{mol/Ns}$) was calculated as the ratio between $VPCr_{\text{stim}}$ and the specific force generated at the start of the fatiguing exercise. Oxidative cost of contraction (Ox_{cost} , in $\mu\text{mol/N*s}$) was calculated at the end of muscle activity as the ratio between $VPCr_{\text{rec}}$ and specific force produced (11) considering that, at this time, ATP production from oxidative phosphorylation is equal to $VPCr_{\text{rec}}$ (49, 55).

Myosin heavy-chain isoforms analysis

Freeze-clamped muscles (50 mg) were homogenized in 600 μl of a solution containing (mM): NaCl 300, NaH_2PO_4 100, Na_2HPO_4 50, $\text{Na}_4\text{P}_2\text{O}_7$ 10, MgCl_2 1, EDTA 10 and β -mercaptoethanol 1.4; pH 6.5. After incubation for 24 h at 4°C, the homogenates were centrifuged (15 min, 13000 x g , 4°C). The supernatants were diluted 1:1 with glycerol and stored at -80°C. Total protein concentrations were measured with the Pierce BCA Protein Assay Kit (Thermo Scientific, Illkirch, France) according to the manufacturer's instructions. Two μg of total proteins were denatured and then subjected to electrophoresis as previously described (8) using a Mini Protean Tetra system (Bio-Rad, Marnes-la-Coquette, France). Gels were run at 72 V for 48 h, stained with IRDye® Blue Protein Stain (LI-COR Biosciences, Lincoln, NE, USA), and then scanned in the 700 nm channel of an infrared imaging system with a 42- μm spatial resolution (Odyssey®, LI-COR Biosciences, Lincoln, NE, USA). MHC isoforms were identified by comparing them with bands of myosin extracts from control soleus muscle (8) and quantified with the ImageJ software (<http://imagej.nih.gov/ij/>).

Intramuscular ATP content

Freeze-clamped muscles (40-60 mg) were homogenized in 1.2 mL of ice-cold perchloric acid (0.6 M). After incubation for 15 min at 4°C, homogenates were centrifuged (15 min, 2000 x g, 4°C). The supernatants were neutralized with K₂CO₃, and placed for 30 min at 4°C. After being centrifuged (15 min, 2000 x g, 4°C) to remove precipitates, the supernatants were aliquoted and stored at -80°C. ATP concentrations were determined using the bioluminescence ATP determination kit (ref. A22066, Invitrogen, Eugene, Oregon, USA) according to the manufacturer's instructions. Luminescence was measured on a microplate reader (Victor X3, PerkinElmer, Waltham, MA, USA). All samples were run in duplicate.

Mitochondrial DNA content

Total genomic DNA was isolated from freeze-clamped gastrocnemius muscle using the Nucleospin Tissue extraction kit (Macherey-Nagel, Düren, Germany). Isolated gDNA was quantified using the Nanovue Plus Spectrophotometer (GE Healthcare, Life Technologies, France). A real time PCR was performed using the SYBR Green PCR Master Mix Protocol (Bio-Rad France, Marnes-la-Coquette, France) in triplicate on the CFX96 Real Time System (BioRad France). A 10 min denaturation step at 94°C was followed by 40 cycles of denaturation at 94°C for 10 s and annealing/extension at 60°C for 30 s. mtDNA content was determined with the mitochondrial cytochrome c oxidase II (COXII) gene expression (forward 5'GCCGACTAAATCAAGCAACA^{3'} and reverse 5'CAATGGGCATAAAGCTATGG^{3'}) normalized to the genomic NADH deshydrogenase uboquinone flavoprotein 1 (Ndufv1) gene (forward 5'CTTCCCCACTGGCCTCAAG^{3'} and reverse 5'CCAAAACCCAGTGATCCAGC^{3'}).

Statistical analysis

Data are expressed as mean ± SE. Statistical analyses were performed using JMP software version 9 (SAS Institute Inc., Cary, NC, USA). Significant differences were

determined by unpaired two-tailed Student's *t*-tests or by two-factor (group × time) analysis of variance (ANOVAs) with repeated measures on time followed, when appropriate, by Tukey-Kramer post-hoc multiple comparison tests for determining pairwise differences between groups. The significance level was set at $P < 0.05$.

RESULTS

Morphological changes

At the end of the 8-week treatment period, body weight and gastrocnemius muscle volume were larger (+29% and +58%, respectively) in animal treated with sActRIIB-Fc (Fig. 1A and 1B). Furthermore, ActRIIB blockade did not alter the proportion of MHC isoforms in the gastrocnemius muscle (Fig. 1C).

Mechanical performance

The force-frequency curve was constructed from data obtained during incremental frequency trains in electrostimulated gastrocnemius muscle (Fig. 2A). As shown in Fig. 2B and 2C, treatment with sActRIIB-Fc did not affect the maximal tetanic force but significantly reduced the maximal specific tetanic force. Besides, there was no difference between both groups for f_{50} , i.e., the electrostimulation frequency for which 50% of the maximal force was exerted (Fig. 2D).

Changes in absolute force production and fatigue resistance during the 6-min in vivo fatiguing exercise are shown in Fig. 3A and 3B. Absolute force transiently increased in the early stage of the exercise to reach a maximal value (F_{\max}); F_{\max} and force increase ($F_{\max} - F_{\text{start}}$) were larger (+26% and +33%, respectively) in animals receiving sActRIIB-Fc (Fig. 3C and 3D). Afterward, force progressively decreased until the end of the exercise as a sign of fatigue

development (Fig. 3A). Interestingly, fatigue resistance became significantly lower in sActRIIB-Fc treated animals from the middle of the exercise (Fig. 3B). At the end of the exercise, the extent of force reduction was larger in animals treated with sActRIIB-Fc (68 ± 4 % vs. 50 ± 4 %; Fig. 3B). Overall, total force produced during the whole fatiguing exercise was 12% larger in the group receiving sActRIIB-Fc (Fig. 3E). Besides, the shape of specific force curve during the fatiguing exercise was similar between both groups (Fig. 4A). Nevertheless, maximal specific force (Fig. 4B) and total specific force produced during the whole fatiguing exercise (Fig. 4C) were significantly lower (-19% and -28%, respectively) in sActRIIB-Fc treated animals.

Bioenergetics

In resting gastrocnemius muscle, there were no differences between both groups for [PCr]/[ATP] ratio, $[P_i]$ and [ATP] (Table 1). On the contrary, [PCr], [ADP] and pH were significantly lower in animals treated with sActRIIB-Fc. Importantly, the mitochondrial DNA copy numbers remained largely unchanged following sActRIIB treatment (Fig. 5).

At the start of the fatiguing exercise, PCr was rapidly consumed (Fig. 6A) at a similar rate between both groups (Fig. 7A) and PCr cost of contraction was not affected by sActRIIB-Fc treatment (Fig. 7B). In the middle of the exercise, [PCr] reached a steady state that remained stable until the end of the contractile session (Fig. 6A), when the extent of PCr degradation ($\Delta[PCr]$) did not differ between both groups (Table 1). For each animal, P_i accumulated throughout the fatiguing exercise with an initial phase of rapid and massive accumulation followed by a phase of steady state (Fig. 6B) whereas [ATP] remained close to its basal value during the whole exercise (Fig. 6C). At the end of the exercise, there were no differences between PBS and sActRIIB-Fc groups for $[P_i]$ and $\Delta[ATP]$ (Table 1). The time-course of intracellular pH was also strongly similar between both groups, with a rapid acidosis early in the exercise, followed by a phase of steady state that remained fairly constant until the cessation of electrostimulation (Fig. 6D). At that time, the extent of acidosis was not

affected by sActRIIB-Fc treatment (Table 1). Besides, the oxidative cost of contraction did not differ between both groups (Fig. 7C) but the maximal rate of oxidative ATP synthesis (Q_{\max}) was 44% lower in animals treated with sActRIIB-Fc (Fig. 7D).

During the recovery period following the fatiguing exercise, phosphorylated compound levels and pH progressively returned toward their respective basal values (Fig. 6A, 6B, 6C and 6D). Noteworthy, the initial rate of PCr resynthesis and proton efflux were lower (-34% and -92%, respectively) in animals treated with sActRIIB-Fc (Fig. 7E and 7F).

DISCUSSION

This study is the first attempt for investigating in vivo the effect of long-term ActRIIB signaling blockade on muscle anatomy, energy metabolism and force-generating capacity. We mainly found that ActRIIB blockade (i) impairs oxidative mitochondrial function while (ii) absolute force generation is increased and (iii) specific force and fatigue resistance are both reduced. Despite these abnormalities, the bioenergetics status throughout a fatiguing bout of exercise was not altered.

One of the major findings of the current study is that long-term disruption of ActRIIB signaling impairs mitochondrial function in skeletal muscle, which is comparable to data obtained in myostatin-deficient animals (2, 6, 19, 45). We found actually that sActRIIB-Fc treatment dramatically reduced the maximal rate of oxidative ATP synthesis (-42%), which is considered as a robust and highly reproducible in vivo index of oxidative mitochondrial capacity that has been widely used in research and clinical applications (4, 7, 26, 32). Our findings are in agreement with previous in vitro experiments conducted in wild-type mice showing that sActRIIB-Fc delivery reduces the expression of genes involved in mitochondrial oxidative phosphorylation (50, 60) and decreases the level of porin, a mitochondrial membrane protein involved in the transport of ATP between mitochondrial matrix and cytosol (52).

Nevertheless, in agreement with previous experiments in soleus and EDL muscles from healthy mice treated with sActRIIB-Fc (52), we measured that the mitochondrial DNA copy number in gastrocnemius muscle remained largely unchanged following sActRIIB treatment, hence indicating that the mitochondrial impairment was not caused by any decreased mitochondria content. Besides, it must be kept in mind that the ability of mitochondria to produce ATP critically depends on oxygen supply. Interestingly, we observed that pH and PCr level were both significantly lower in resting hypertrophied muscle. This indicates that sActRIIB-Fc limits muscle oxygen availability given that the combination of intracellular acidosis and PCr depletion is an indicator of basal muscle hypoxia (12). Accordingly, we found that proton efflux at the start of the postexercise period was significantly slower in mice treated with soluble ActRIIB, hence leading to assume that the hypoxic state might be due to decreased tissue perfusion. Our assumption is consistent with previous histological analyses showing that muscle capillarity is reduced in normal mice receiving a 4-month sActRIIB-Fc treatment (52) and in myostatin-deficient muscle (2, 51). Consequently, it is possible that sActRIIB-Fc limits oxygen delivery to the muscle, which in return would reduce mitochondrial respiration. Noteworthy, we found that sActRIIB-Fc treatment did not alter basal ATP level but reduced that of ADP. Considering the CK reaction that reversely transfers high-energy phosphate from PCr to ADP to form ATP via the reaction: $\text{PCr} + \text{ADP} + \text{H}^+ \leftrightarrow \text{ATP} + \text{creatine}$ (34), the reduced ADP level could be interpreted as a compensatory mechanism allowing to maintain ATP homeostasis in the face of both an intracellular acidosis and a reduced PCr content.

The mouse gastrocnemius muscle is predominantly glycolytic. However, considering that energy metabolism plays a critical role in muscle contraction, one can now ask whether the mitochondrial impairment induced by ActRIIB blockade causes functional alteration in exercising muscle, i.e., when energy demand is substantially larger. This question is legitimate given the contrasting effect of sActRIIB-Fc on mechanical performance. Firstly, we shown that force increase ($F_{\text{max}} - F_{\text{start}}$) and both maximal (F_{max}) and total absolute force produced during the 6-min in vivo fatiguing exercise were larger in animals treated with sActRIIB-Fc, which is

in line with previous studies showing an increased forelimb grip strength in normal mice receiving sActRIIB-Fc (1, 33). Importantly, our findings confirm that sActRIIB-Fc treatment might be beneficial for patients suffering from muscle wasting. Secondly, our results related to the specific force clearly indicated that the mechanical performance was reduced as compared to what could have been expected on the basis of the muscle hypertrophy. Actually, we showed that muscle hypertrophy was not accompanied by a proportional increase in absolute force. On the contrary, specific force was reduced in animals treated with sActRIIB-Fc in agreement with what has been already reported in hypertrophied muscle of myostatin-deficient mice (2, 19, 42). Thirdly, we observed that sActRIIB-Fc treatment did not improve maximal tetanic force in vivo. Although counterintuitive, this finding has been already reported in isolated muscles from myostatin-deficient mice (2) or from wild-type mice treated with sActRIIB-Fc (1, 15) or myostatin neutralizing antibodies (36). While the underlying cause for this phenomenon has not been documented, one must be aware that myostatin deficiency reduces the relative collagen content, which alters muscle mechanistic by increasing the stiffness of muscle aponeurosis and tendon (43, 59). It is then conceivable that the long-term ActRIIB blockade produces similar alterations, hence ultimately lowering the ability to generate tetanic tension. Lastly, we found that ActRIIB signaling inhibition reduced fatigue resistance during the in vivo fatiguing exercise, which corroborates other studies showing that sActRIIB-Fc delivery increases fatigability in hindlimb muscle electrically stimulated in situ (15) and decreases the time to exhaustion during incremental speed running tests (52).

Despite the mitochondrial and mechanical abnormalities reported herein, several lines of evidence led us to believe that sActRIIB-Fc treatment is not deleterious for energy metabolism in exercising muscle. Intramyofibrillar PCr concentration is controlled by the CK reaction and the PCr-CK system is considered to have a crucial role in ATP homeostasis during exercise. The system actually functions as an energy buffer at the transition from rest to exercise and – with continuation of exercise – as an energy carrier directly involved in the transport of high-energy phosphate between the sites of production (mitochondrial matrix) and utilization (cytosol) of ATP (24). In the present study, sActRIIB-Fc treatment did alter neither

the initial rate of PCr degradation nor the PCr cost of contraction at the start of the fatiguing exercise, thereby indicating that the energy buffering function of the PCr-CK system remained unaffected. At the end of the exercise, there were no differences between both groups for oxidative cost of contraction and extents of both PCr consumption and [ATP] reduction, which demonstrates that (i) sActRIIB-Fc treatment does not alter the energy transport function of the PCr-CK system and (ii) energy metabolism entirely fits ATP demand for contraction. Also, it is noteworthy that the time-dependent changes in pH during the fatiguing exercise were similar between both groups. Considering that intracellular acidosis in contracting muscle mainly reflects glycolytic flux, our data suggests that glucose metabolism was not disturbed by ActRIIB blockade, which is in line with previous experiments showing that sActRIIB-Fc treatment does affect neither muscle glucose uptake (1) nor transcription of gene involved in glucose metabolism (52). Overall, one can affirm that the fact that muscle capacity for generating force does not take full advantage of muscle hypertrophy is not due to alteration in energy metabolism, and other mechanism(s) should then occur but this issue has to our knowledge never been documented.

Typological changes, calcium fluxes alteration and muscle architecture changes have been put forward as accounting factors of the increased fatigability and the decreased specific force reported in myostatin-deficient animals (2, 9, 43, 46, 59). In these animals, the relative fraction of glycolytic fibers – which produce more force but conversely are more susceptible to fatigue – is increased at the expense of both oxidative and oxidative-glycolytic fibers (18, 22, 39). We have checked fiber composition in the gastrocnemius muscle and found that ActRIIB blockade did not cause fiber-type conversion, as previously shown in other sActRIIB-Fc treated mouse muscles such as quadriceps, EDL, soleus and plantaris (13, 33, 52). Our finding therefore rules out any typological change as an accounting factor of the altered mechanical performance in sActRIIB-Fc treated muscle. Accumulation of tubular aggregates at the calcium-release channel of the sarcoplasmic reticulum has also been proposed to alter calcium handling during excitation-contraction cycles in myostatin-deficient mice thereby altering mechanical performance (2, 9). Nevertheless, this issue remains unlikely herein

because we found that ActRIIB blockade did not affect f_{50} (the electrostimulation frequency for which 50% of the maximal tetanic force was exerted) an in vivo indicator of calcium sensitivity (21, 54). On the other hand, it is possible that the reduced mechanical capacity in sActRIIB-Fc treated animals was linked to hypertrophy-induced alterations of fiber pennation angles caused by increased muscle cross sectional area. This muscle architecture alteration would thus impair the transmission of force by myofilaments (25, 41).

In conclusion, our study demonstrates in vivo that the pharmacological blockade of ActRIIB impairs mitochondrial function possibly via muscle oxygenation limitation, but this impairment does not compromise bioenergetics status and gastrocnemius muscle function during sustained muscle activity. However, it must be kept in mind that the gastrocnemius muscle is predominantly glycolytic and our results cannot be extrapolated to type I oxidative muscle fiber. On the other hand, it is noteworthy that despite reduced specific force and increased fatigability in the late phase of muscle activity, ActRIIB blockade also increases absolute force-generating capacity. Although fatigue resistance and specific force are important variables of muscle function, patients' performance is usually assessed according to whether they produce enough force to accomplish a short-duration task. In that context, it is obvious that the increased absolute force-generating capacity represents a functional advantage. Therefore, beyond the demonstration that ActRIIB signaling plays key roles in the balance between muscle mass, force generation, oxidative metabolism and resistance to fatigue, our data strengthen ActRIIB blockade as a promising clinical application for muscle wasting disorders.

ACKNOWLEDGEMENTS

We are grateful to Acceleron Pharma Inc. for the gift of sActRIIB-Fc. The authors also thank Ms Laurence Louis (Plate-Forme Génomique et Transcriptomique, Aix-Marseille Université, INSERM, UMR_S910, Marseille, France) for its helpful assistance with infrared imaging.

GRANTS

This work was financially supported by the French Muscular Dystrophy Association (AFM-Téléthon).

DISCLOSURE

The authors have no conflicts of interest, financial or otherwise, to declare. Acceleron Pharma Inc. did not influence data collection, analysis, interpretation and decision to publish the present study.

REFERENCES

1. **Akpan I, Goncalves MD, Dhir R, Yin X, Pistilli EE, Bogdanovich S, Khurana TS, Ucran J, Lachey J, Ahima RS.** The effects of a soluble activin type IIB receptor on obesity and insulin sensitivity. *Int J Obes (Lond)* 33: 1265-1273, 2009.
2. **Amthor H, Macharia R, Navarrete R, Schuelke M, Brown SC, Otto A, Voit T, Muntoni F, Vrbova G, Partridge T, Zammit P, Bungler L, Patel K.** Lack of myostatin results in excessive muscle growth but impaired force generation. *Proc Natl Acad Sci USA* 104: 1835-1840, 2007.
3. **Arnold DL, Bore PJ, Radda GK, Styles P, Taylor DJ.** Excessive intracellular acidosis of skeletal muscle on exercise in a patient with a post-viral exhaustion/fatigue syndrome. A ³¹P nuclear magnetic resonance study. *Lancet* 1: 1367-1369, 1984.
4. **Arnold DL, Matthews PM, Radda GK.** Metabolic recovery after exercise and the assessment of mitochondrial function in vivo in human skeletal muscle by means of ³¹P NMR. *Magn Reson Med* 1: 307-315, 1984.
5. **Attie KM, Borgstein NG, Yang Y, Condon CH, Wilson DM, Pearsall AE, Kumar R, Willins DA, Sehra JS, Sherman ML.** A single ascending-dose study of muscle regulator ACE-031 in healthy volunteers. *Muscle Nerve* 47: 416-423, 2013.
6. **Baligand C, Gilson H, Menard JC, Schakman O, Wary C, Thissen JP, Carlier PG.** Functional assessment of skeletal muscle in intact mice lacking myostatin by concurrent NMR imaging and spectroscopy. *Gene Ther* 17: 328-337, 2009.
7. **Bendahan D, Desnuelle C, Vanuxem D, Confort-Gouny S, Figarella-Branger D, Pellissier JF, Kozak-Ribbens G, Pouget J, Serratrice G, Cozzone PJ.** ³¹P NMR spectroscopy and ergometer exercise test as evidence for muscle oxidative performance improvement with coenzyme Q in mitochondrial myopathies. *Neurology* 42: 1203-1208, 1992.

8. **Birot OJ, Koulmann N, Peinnequin A, Bigard XA.** Exercise-induced expression of vascular endothelial growth factor mRNA in rat skeletal muscle is dependent on fibre type. *J Physiol* 552: 213-221, 2003.
9. **Bodnar D, Geyer N, Ruzsnavszky O, Olah T, Hegyi B, Sztretye M, Fodor J, Dienes B, Balogh A, Papp Z, Szabo L, Muller G, Csernoch L, Szentesi P.** Hypermuscular mice with mutation in the myostatin gene display altered calcium signalling. *J Physiol (Lond)* 592: 1353-1365, 2014.
10. **Bogdanovich S, Krag TO, Barton ER, Morris LD, Whittemore LA, Ahima RS, Khurana TS.** Functional improvement of dystrophic muscle by myostatin blockade. *Nature* 420: 418-421, 2002.
11. **Boska M.** Estimating the ATP cost of force production in the human gastrocnemius/soleus muscle group using ³¹P MRS and ¹H MRI. *NMR Biomed* 4: 173-181, 1991.
12. **Boutillier RG.** Mechanisms of cell survival in hypoxia and hypothermia. *J Exp Biol* 204: 3171-3181, 2001.
13. **Cadena SM, Tomkinson KN, Monnell TE, Spaits MS, Kumar R, Underwood KW, Pearsall RS, Lachey JL.** Administration of a soluble activin type IIB receptor promotes skeletal muscle growth independent of fiber type. *J Appl Physiol (1985)* 109: 635-642, 2010.
14. **Cea G, Bendahan D, Manners D, Hilton-Jones D, Lodi R, Styles P, Taylor DJ.** Reduced oxidative phosphorylation and proton efflux suggest reduced capillary blood supply in skeletal muscle of patients with dermatomyositis and polymyositis: a quantitative ³¹P-magnetic resonance spectroscopy and MRI study. *Brain* 125: 1635-1645, 2002.
15. **Chiu CS, Peekhaus N, Weber H, Adamski S, Murray EM, Zhang HZ, Zhao JZ, Ernst R, Lineberger J, Huang L, Hampton R, Arnold BA, Vitelli S, Hamuro L, Wang WR, Wei N, Dillon GM, Miao J, Alves SE, Glantschnig H, Wang F, Wilkinson HA.** Increased muscle force production and bone mineral density in ActRIIB-Fc-treated mature rodents. *J Gerontol A Biol Sci Med Sci* 68: 1181-1192, 2013.

16. **De Caestecker M.** The transforming growth factor-beta superfamily of receptors. *Cytokine Growth Factor Rev* 15: 1-11, 2004.
17. **Dumonceaux J, Amthor H.** Current advances in the development of therapies for neuromuscular disorders based on myostatin signalling, 3rd International Institute of Myology Workshop, Paris, September 12th, 2008. *Neuromuscul Disord* 19: 797-799, 2009.
18. **Gentry BA, Ferreira JA, Phillips CL, Brown M.** Hindlimb skeletal muscle function in myostatin-deficient mice. *Muscle Nerve* 43: 49-57, 2011.
19. **Giannesini B, Vilmen C, Amthor H, Bernard M, Bendahan D.** Lack of myostatin impairs mechanical performance and ATP cost of contraction in exercising mouse gastrocnemius muscle in vivo. *Am J Physiol Endocrinol Metab* 305: E33-40, 2013.
20. **Giannesini B, Vilmen C, Le Fur Y, Dalmasso C, Cozzone PJ, Bendahan D.** A strictly noninvasive MR setup dedicated to longitudinal studies of mechanical performance, bioenergetics, anatomy, and muscle recruitment in contracting mouse skeletal muscle. *Magn Reson Med* 64: 262-270, 2010.
21. **Gineste C, Le Fur Y, Vilmen C, Le Troter A, Pecchi E, Cozzone PJ, Hardeman EC, Bendahan D, Gondin J.** Combined MRI and ³¹P-MRS investigations of the ACTA1(H40Y) mouse model of nemaline myopathy show impaired muscle function and altered energy metabolism. *PLoS One* 8: e61517, 2013.
22. **Girgenrath S, Song K, Whittemore LA.** Loss of myostatin expression alters fiber-type distribution and expression of myosin heavy chain isoforms in slow- and fast-type skeletal muscle. *Muscle Nerve* 31: 34-40, 2005.
23. **Goodwill AG, Frisbee JC.** Oxidant stress and skeletal muscle microvasculopathy in the metabolic syndrome. *Vascul Pharmacol* 57: 150-159, 2012.
24. **Hochachka PW, McClelland GB.** Cellular metabolic homeostasis during large-scale change in ATP turnover rates in muscles. *J Exp Biol* 200: 381-386, 1997.
25. **Hughes DC, Wallace MA, Baar K.** Effects of aging, exercise, and disease on force transfer in skeletal muscle. *Am J Physiol Endocrinol Metab* 309: E1-E10, 2015.

26. **Kemp GJ, Ahmad RE, Nicolay K, Prompers JJ.** Quantification of skeletal muscle mitochondrial function by ^{31}P magnetic resonance spectroscopy techniques: a quantitative review. *Acta Physiol (Oxf)* 213: 107-144, 2015.
27. **Kemp GJ, Hands LJ, Ramaswami G, Taylor DJ, Nicolaides A, Amato A, Radda GK.** Calf muscle mitochondrial and glycogenolytic ATP synthesis in patients with claudication due to peripheral vascular disease analysed using ^{31}P magnetic resonance spectroscopy. *Clin Sci (Lond)* 89: 581-590, 1995.
28. **Kemp GJ, Radda GK.** Quantitative interpretation of bioenergetic data from ^{31}P and ^1H magnetic resonance spectroscopic studies of skeletal muscle: an analytical review. *Magn Reson Q* 10: 43-63, 1994.
29. **Kemp GJ, Thompson CH, Sanderson AL, Radda GK.** pH control in rat skeletal muscle during exercise, recovery from exercise, and acute respiratory acidosis. *Magn Reson Med* 31: 103-109, 1994.
30. **Krivickas LS, Walsh R, Amato AA.** Single muscle fiber contractile properties in adults with muscular dystrophy treated with MYO-029. *Muscle Nerve* 39: 3-9, 2009.
31. **Lach-Trifilieff E, Minetti GC, Sheppard K, Ibebunjo C, Feige JN, Hartmann S, Brachat S, Rivet H, Koelbing C, Morvan F, Hatakeyama S, Glass DJ.** An antibody blocking activin type II receptors induces strong skeletal muscle hypertrophy and protects from atrophy. *Mol Cell Biol* 34: 606-618, 2014.
32. **Lanza IR, Bhagra S, Nair KS, Port JD.** Measurement of human skeletal muscle oxidative capacity by ^{31}P -MR spectroscopy: a cross-validation with in vitro measurements. *J Magn Reson Imaging* 34: 1143-1150, 2011.
33. **Lawlor MW, Read BP, Edelstein R, Yang N, Pierson CR, Stein MJ, Wermer-Colan A, Buj-Bello A, Lachey JL, Seehra JS, Beggs AH.** Inhibition of activin receptor type IIB increases strength and lifespan in myotubularin-deficient mice. *Am J Pathol* 178: 784-793, 2011.

34. **Lawson JW, Veech RL.** Effects of pH and free Mg²⁺ on the Keq of the creatine kinase reaction and other phosphate hydrolyses and phosphate transfer reactions. *J Biol Chem* 254: 6528-6537, 1979.
35. **Le Fur Y, Nicoli F, Guye M, Confort-Gouny S, Cozzone PJ, Kober F.** Grid-free interactive and automated data processing for MR chemical shift imaging data. *Magma* 23: 23-30, 2010.
36. **LeBrasseur NK, Schelhorn TM, Bernardo BL, Cosgrove PG, Loria PM, Brown TA.** Myostatin inhibition enhances the effects of exercise on performance and metabolic outcomes in aged mice. *J Gerontol A Biol Sci Med Sci* 64: 940-948, 2009.
37. **Lee SJ, McPherron AC.** Regulation of myostatin activity and muscle growth. *Proc Natl Acad Sci USA* 98: 9306-9311, 2001.
38. **Lee SJ, Reed LA, Davies MV, Girgenrath S, Goad ME, Tomkinson KN, Wright JF, Barker C, Ehrmantraut G, Holmstrom J, Trowell B, Gertz B, Jiang MS, Sebald SM, Matzuk M, Li E, Liang LF, Quattlebaum E, Stotish RL, Wolfman NM.** Regulation of muscle growth by multiple ligands signaling through activin type II receptors. *Proc Natl Acad Sci USA* 102: 18117-18122, 2005.
39. **Matsakas A, Mouisel E, Amthor H, Patel K.** Myostatin knockout mice increase oxidative muscle phenotype as an adaptive response to exercise. *J Muscle Res Cell Motil* 31: 111-125, 2010.
40. **Mattei JP, Fur YL, Cuge N, Guis S, Cozzone PJ, Bendahan D.** Segmentation of fascias, fat and muscle from magnetic resonance images in humans: the DISPIMAG software. *Magma* 19: 275-279, 2006.
41. **Maxwell LC, Faulkner JA, Hyatt GJ.** Estimation of number of fibers in guinea pig skeletal muscles. *J Appl Physiol (1985)* 37: 259-264, 1974.
42. **Mendias CL, Kayupov E, Bradley JR, Brooks SV, Claflin DR.** Decreased specific force and power production of muscle fibers from myostatin-deficient mice are associated with a suppression of protein degradation. *J Appl Physiol (1985)* 111: 185-191, 2011.

43. **Mendias CL, Marcin JE, Calderon DR, Faulkner JA.** Contractile properties of EDL and soleus muscles of myostatin-deficient mice. *J Appl Physiol* 101: 898-905, 2006.
44. **Morrison BM, Lachey JL, Warsing LC, Ting BL, Pullen AE, Underwood KW, Kumar R, Sako D, Grinberg A, Wong V, Colantuoni E, Sehra JS, Wagner KR.** A soluble activin type IIB receptor improves function in a mouse model of amyotrophic lateral sclerosis. *Exp Neurol* 217: 258-268, 2009.
45. **Mouisel E, Relizani K, Mille-Hamard L, Denis R, Hourde C, Agbulut O, Patel K, Arandel L, Morales-Gonzalez S, Vignaud A, Garcia L, Ferry A, Luquet S, Billat V, Ventura-Clapier R, Schuelke M, Amthor H.** Myostatin is a key mediator between energy metabolism and endurance capacity of skeletal muscle. *Am J Physiol Regul Integr Comp Physiol* 307: R444-454, 2014.
46. **Personius KE, Jayaram A, Krull D, Brown R, Xu T, Han B, Burgess K, Storey C, Shah B, Tawil R, Welle S.** Grip force, EDL contractile properties, and voluntary wheel running after postdevelopmental myostatin depletion in mice. *J Appl Physiol* 109: 886-894, 2010.
47. **Pistilli EE, Bogdanovich S, Goncalves MD, Ahima RS, Lachey J, Sehra J, Khurana T.** Targeting the activin type IIB receptor to improve muscle mass and function in the mdx mouse model of Duchenne muscular dystrophy. *Am J Pathol* 178: 1287-1297, 2011.
48. **Ploquin C, Chabi B, Fouret G, Vernus B, Feillet-Coudray C, Coudray C, Bonniou A, Ramonatxo C.** Lack of myostatin alters intermyofibrillar mitochondria activity, unbalances redox status, and impairs tolerance to chronic repetitive contractions in muscle. *Am J Physiol Endocrinol Metab* 302: E1000-1008, 2012.
49. **Radda GK.** The use of NMR spectroscopy for the understanding of disease. *Science* 233: 640-645, 1986.
50. **Rahimov F, King OD, Warsing LC, Powell RE, Emerson CP, Jr., Kunkel LM, Wagner KR.** Gene expression profiling of skeletal muscles treated with a soluble activin type IIB receptor. *Physiol Genomics* 43: 398-407, 2011.

51. **Rehfeldt C, Ott G, Gerrard DE, Varga L, Schlote W, Williams JL, Renne U, Bunker L.** Effects of the compact mutant myostatin allele Mstn (Cmpt-dl1Abc) introgressed into a high growth mouse line on skeletal muscle cellularity. *J Muscle Res Cell Motil* 26: 103-112, 2005.
52. **Relizani K, Mouisel E, Giannesini B, Hourde C, Patel K, Morales Gonzalez S, Julich K, Vignaud A, Pietri-Rouxel F, Fortin D, Garcia L, Blot S, Ritvos O, Bendahan D, Ferry A, Ventura-Clapier R, Schuelke M, Amthor H.** Blockade of ActRIIB signaling triggers muscle fatigability and metabolic myopathy. *Mol Ther* 22: 1423-1433, 2014.
53. **Roth K, Weiner MW.** Determination of cytosolic ADP and AMP concentrations and the free energy of ATP hydrolysis in human muscle and brain tissues with ³¹P NMR spectroscopy. *Magn Reson Med* 22: 505-511, 1991.
54. **Russ DW, Ruggeri RG, Thomas JS.** Central activation and force-frequency responses of the lumbar extensor muscles. *Med Sci Sports Exerc* 41: 1504-1509, 2009.
55. **Taylor DJ, Styles P, Matthews PM, Arnold DA, Gadian DG, Bore P, Radda GK.** Energetics of human muscle: exercise-induced ATP depletion. *Magn Reson Med* 3: 44-54, 1986.
56. **Vanhamme L, van den Boogaart A, Van Huffel S.** Improved method for accurate and efficient quantification of MRS data with use of prior knowledge. *J Magn Reson* 129: 35-43, 1997.
57. **Wagner KR, Fleckenstein JL, Amato AA, Barohn RJ, Bushby K, Escolar DM, Flanigan KM, Pestronk A, Tawil R, Wolfe GI, Eagle M, Florence JM, King WM, Pandya S, Straub V, Juneau P, Meyers K, Csimma C, Araujo T, Allen R, Parsons SA, Wozney JM, Lavallie ER, Mendell JR.** A phase I/II trial of MYO-029 in adult subjects with muscular dystrophy. *Ann Neurol* 63: 561-571, 2008.
58. **Wang Q, McPherron AC.** Myostatin inhibition induces muscle fibre hypertrophy prior to satellite cell activation. *J Physiol (Lond)* 590: 2151-2165, 2012.
59. **Welle S, Cardillo A, Zanche M, Tawil R.** Skeletal muscle gene expression after myostatin knockout in mature mice. *Physiol Genomics* 38: 342-350, 2009.

60. **Zhao B, Li EJ, Wall RJ, Yang J.** Coordinated patterns of gene expressions for adult muscle build-up in transgenic mice expressing myostatin propeptide. *BMC Genomics* 10: 305, 2009.

FIGURE LEGENDS

Figure 1. Effect of a 8-week treatment with PBS or sActRIIB-Fc on body weight (A), gastrocnemius muscle volume (B) and relative distribution of MHC isoform proteins (C). Representative blot depicting the electrophoretic separation of gastrocnemius muscle MHC isoforms (D), which were identified by comparing them with bands of myosin extracts from control soleus muscle. Data are means \pm SE. * Significantly different from PBS.

Figure 2. Absolute force produced during the in vivo force-frequency protocol in gastrocnemius muscle (A). Treatment with sActRIIB-Fc did not affect the maximal tetanic force (B) but reduced the maximal specific tetanic force (C). Besides, there was no difference between both groups for f_{50} (D), which represents the electrostimulation frequency for which 50% of the maximal force was exerted. Data are means \pm SE. * Significantly different from PBS.

Figure 3. Changes in absolute force production (A) and fatigue resistance (B) throughout the 6-min in vivo fatiguing exercise performed simultaneously to metabolic MR acquisition. Maximal force (F_{max} ; panel C), force increase ($F_{max}-F_{start}$; panel D) and the total amount of force produced during the whole exercise (E) were larger (+26%, +33% and +12%, respectively) in animals treated with sActRIIB-Fc. Data are means \pm SE. P_{Anova} indicates the overall result of the two-way repeated measures ANOVA; when justified (P -value < 0.05), Tukey post-hoc multiple comparisons were used for determining pairwise time-points differences. * Significantly different between both groups.

Figure 4. Changes in specific force production throughout the 6-min in vivo fatiguing exercise performed simultaneously to metabolic MR acquisition (A). Maximal specific force (B) and the total amount of specific force produced during the whole exercise (C) were lower in animals treated with sActRIIB-Fc. Data are means \pm SE. P_{Anova} indicates the overall result of the two-

way repeated measures ANOVA; Tukey post-hoc multiple comparisons indicate a significant difference between both groups at each time point. * Significantly different from PBS.

Figure 5. Effect of a 8-week treatment with PBS or sActRIIB-Fc on gastrocnemius muscle mitochondrial DNA content expressed as the cytochrome c oxidase II (COXII) relative copy numbers normalized to NADH deshydrogenase uboquinone flavoprotein 1 (Ndufv1) genomic DNA copies. Data are means \pm SE.

Figure 6. In vivo changes in gastrocnemius muscle [PCr] (A), [P_i] (B), [ATP] (C) and pH (D) during the 6-min fatiguing exercise and the 15-min recovery period. For each panel, the first time point (t = 0) indicates the basal value. Data are means \pm SE.

Figure 7. Initial rate of PCr consumption (A) and PCr cost of contraction (B) at the start of the fatiguing exercise, oxidative cost of contraction (C), maximal rate of oxidative ATP synthesis (D), and initial rate of PCr resynthesis (E) and proton efflux (F) at the start of the recovery period. Data are means \pm SE. * Significantly different from PBS.

Table 1

Effect of a 8-week treatment period with PBS or sActRIIB-Fc on mouse gastrocnemius bioenergetics assessed in vivo using ³¹P-MR spectroscopy.

	PBS	sActRIIB-Fc
<i>Basal</i>		
[PCr]/[ATP]	2.52 ± 0.10	2.47 ± 0.07
[PCr], mM	13.2 ± 0.5	11.6 ± 0.3*
[ATP], mM	5.1 ± 0.2	4.7 ± 0.2
[P _i], mM	2.1 ± 0.3	2.8 ± 0.4
[ADP], μM	6.2 ± 0.6	4.5 ± 0.1*
pH	7.04 ± 0.04	6.95 ± 0.01*
<i>End of the 6-min fatiguing exercise</i>		
Δ[PCr] (relative to basal), mM	8.6 ± 0.7	8.8 ± 0.5
Δ[ATP] (relative to basal), mM	0.49 ± 0.12	0.63 ± 0.21
[P _i], mM	11.2 ± 0.7	12.3 ± 0.6
[ADP], μM	27 ± 4	32 ± 3
ΔpH (relative to basal), pH unit	0.47 ± 0.05	0.46 ± 0.05

Data are means ± SE. * Significantly different from PBS.

Figure 1

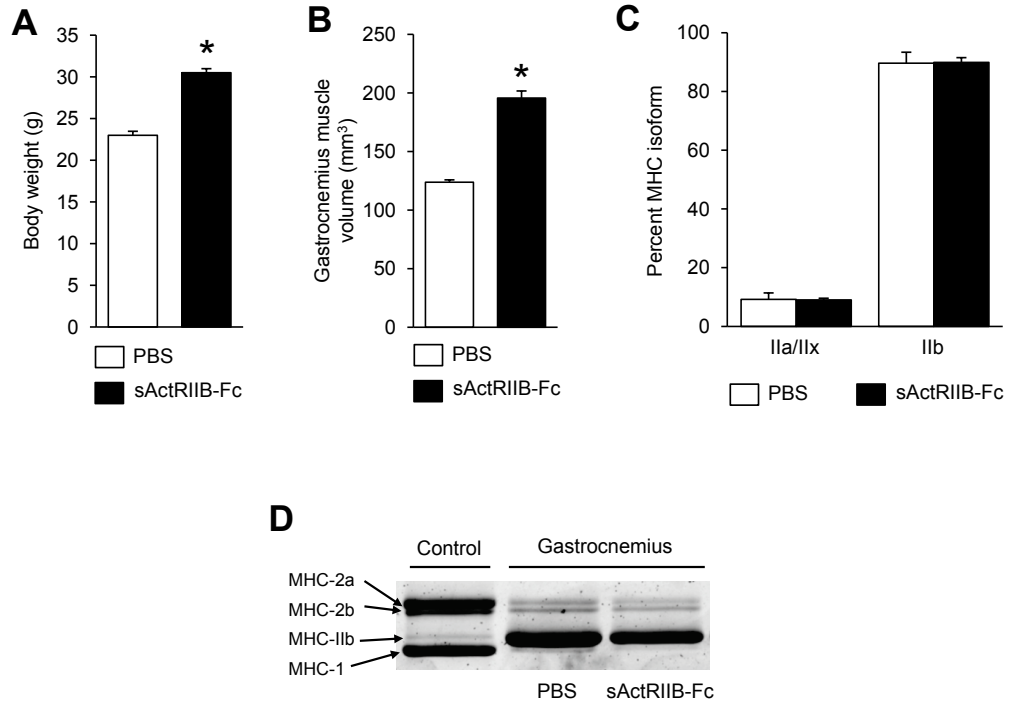


Figure 2

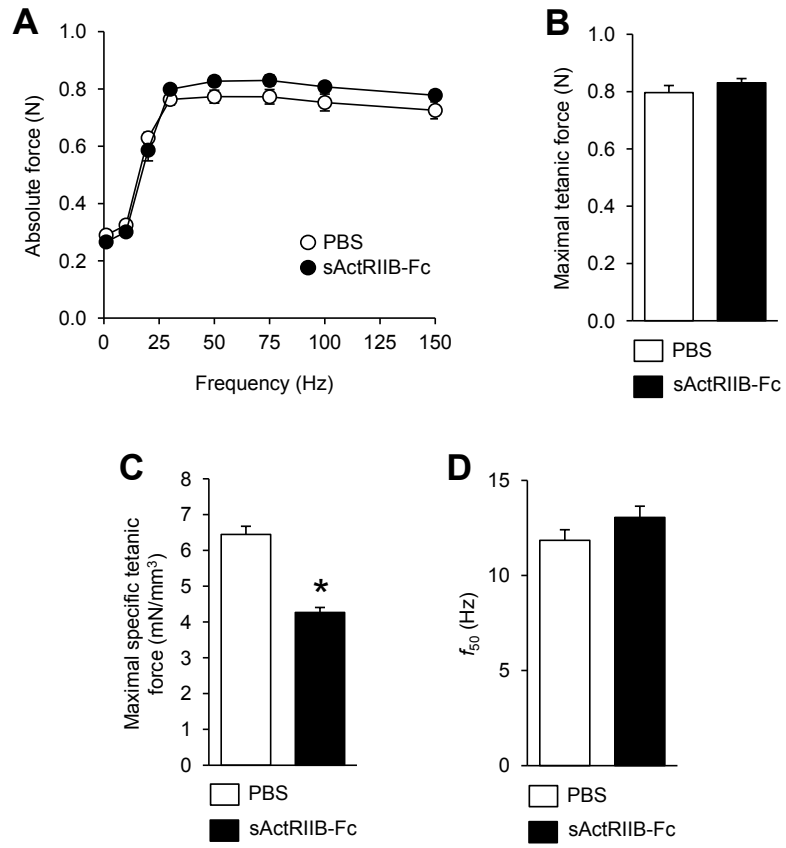


Figure 3

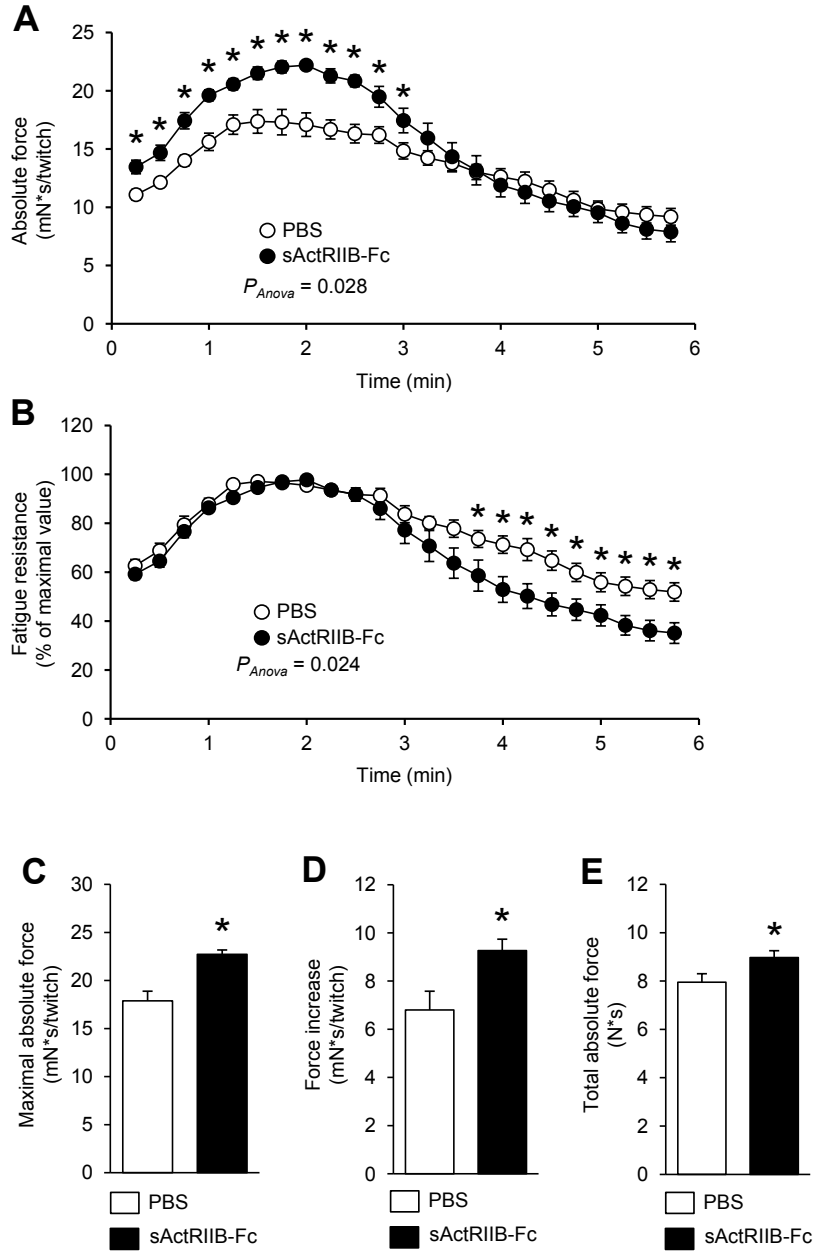


Figure 4

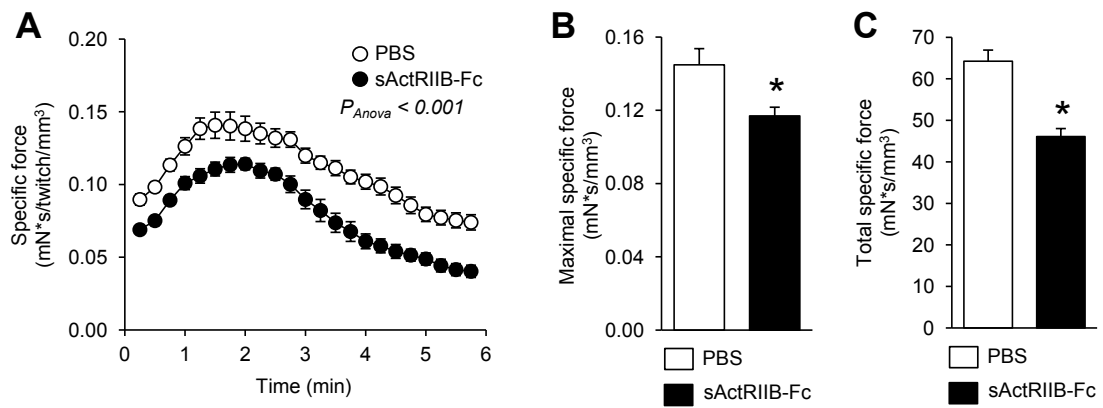


Figure 5

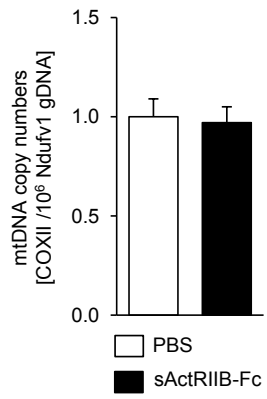


Figure 6

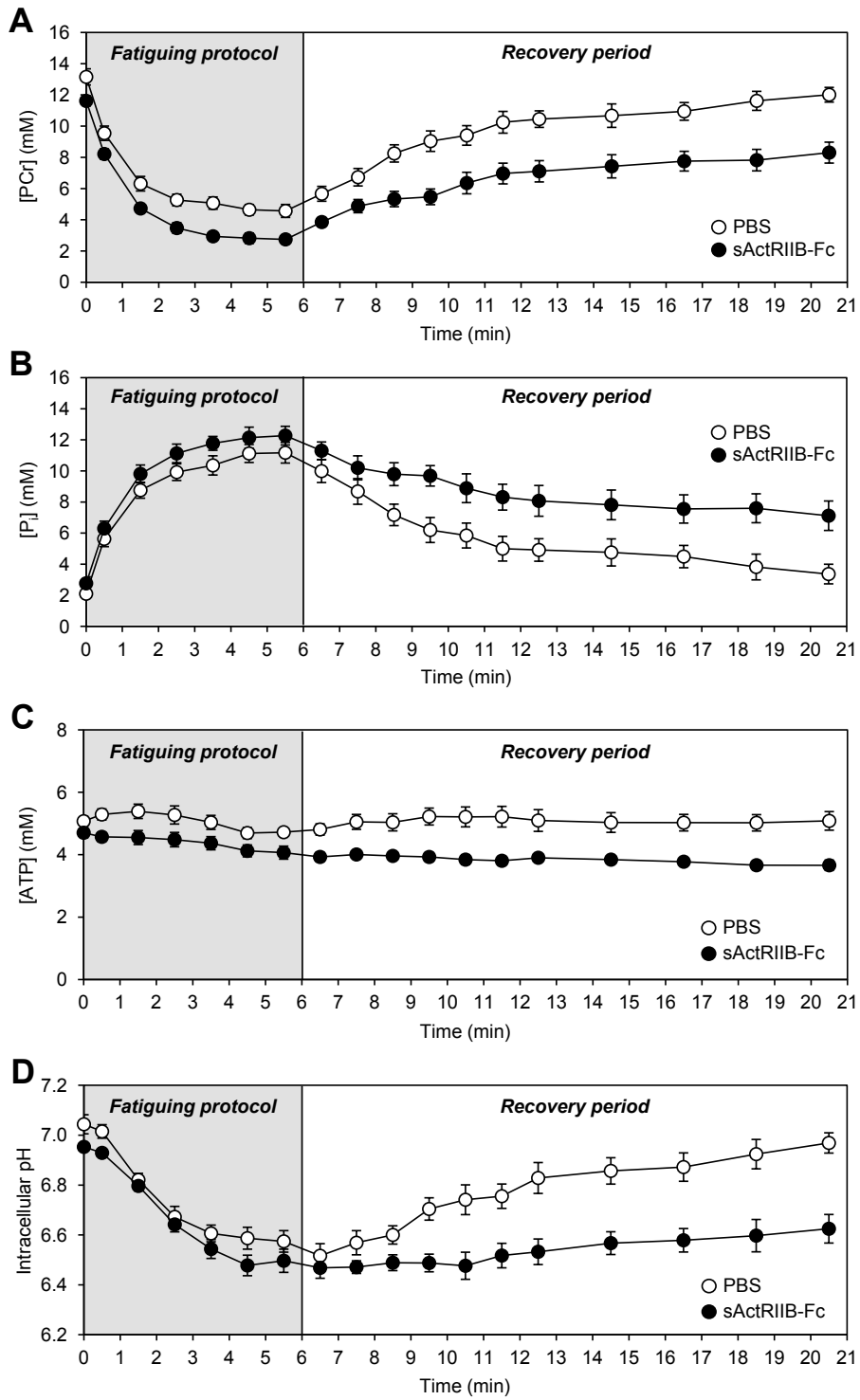


Figure 7

